

# Near-Field to Near/Far-Field Transformation for Arbitrary Near-Field Geometry, Utilizing an Equivalent Magnetic Current

Ardalan Taaghola and Tapan K. Sarkar

**Abstract**—A method is presented for computing near- and far-field patterns of an antenna from its near-field measurements taken over an arbitrary geometry. This method utilizes near-field data to determine an equivalent magnetic current source over a fictitious surface which encompasses the antenna. This magnetic current, once determined, can be used to ascertain the near and the far fields. This method demonstrates that once the values of the electromagnetic field are known over an arbitrary geometry, its values for any other region can be obtained. An electric field integral equation is developed to relate the near fields to the equivalent magnetic current. A moment method procedure is employed to solve the integral equation by transforming it into a matrix equation. A least squares solution via singular value decomposition is used to solve the matrix equation. Computations with both synthetic and experimental data, where the near field of several antenna configurations are measured over various geometric surfaces, illustrate the accuracy of this method.

## I. INTRODUCTION

Presented here is a method for near-field to near/far field transformation which requires no specific geometry for near-field measurements. In this approach, by using the equivalence principle [1], an equivalent magnetic current replaces the radiating antenna. Furthermore, it is assumed that the near field is produced by the equivalent magnetic current and therefore, via Maxwell's equation from the measured near-field data, the current source can be determined. Once this is accomplished, the near field and the far field of the radiating antenna in all regions in space in front of the radiating antenna can be determined directly from the equivalent magnetic current.

An electric field integral equation is developed which pertains to the measured near fields and the equivalent magnetic current. This integral equation has been solved for the unknown magnetic current source through a moment method procedure [2] with point matching, where the equivalent current is expanded as linear combinations of two-dimensional (2-D) pulse basis functions and, therefore, the integral equation is then transformed into a matrix equation. In general, the matrix is rectangular whose dimensions depend on the number of field and source points chosen. The matrix equation is solved by the method of least squares via the singular value decomposition [3], [4]. By this, the moment matrix is decomposed into a set of orthogonal matrices which can be easily inverted.

Another aspect of this approach is that the numerical integrations in the process of creating the moment matrix elements have been avoided by taking a limiting case. Since the field points and the source points are to never coincide, and if their distances are much larger than the sizes of the current patches, then the pulse basis functions expanding the current source can be approximated by Hertzian dipoles [5].

The formulation and theoretical basis for the equivalent magnetic current approach along with the formation of the corresponding matrix equation using the method of moments and its solution using

Manuscript received February 9, 1995; revised January 29, 1996. This work was supported in part by E. I. Dupont de Nemours and Company and by the CASE Center of Syracuse University.

The authors are with the Department of Electrical and Computer Engineering, Syracuse University, Syracuse, NY 13244 USA.

Publisher Item Identifier S 0018-9375(96)03860-4.

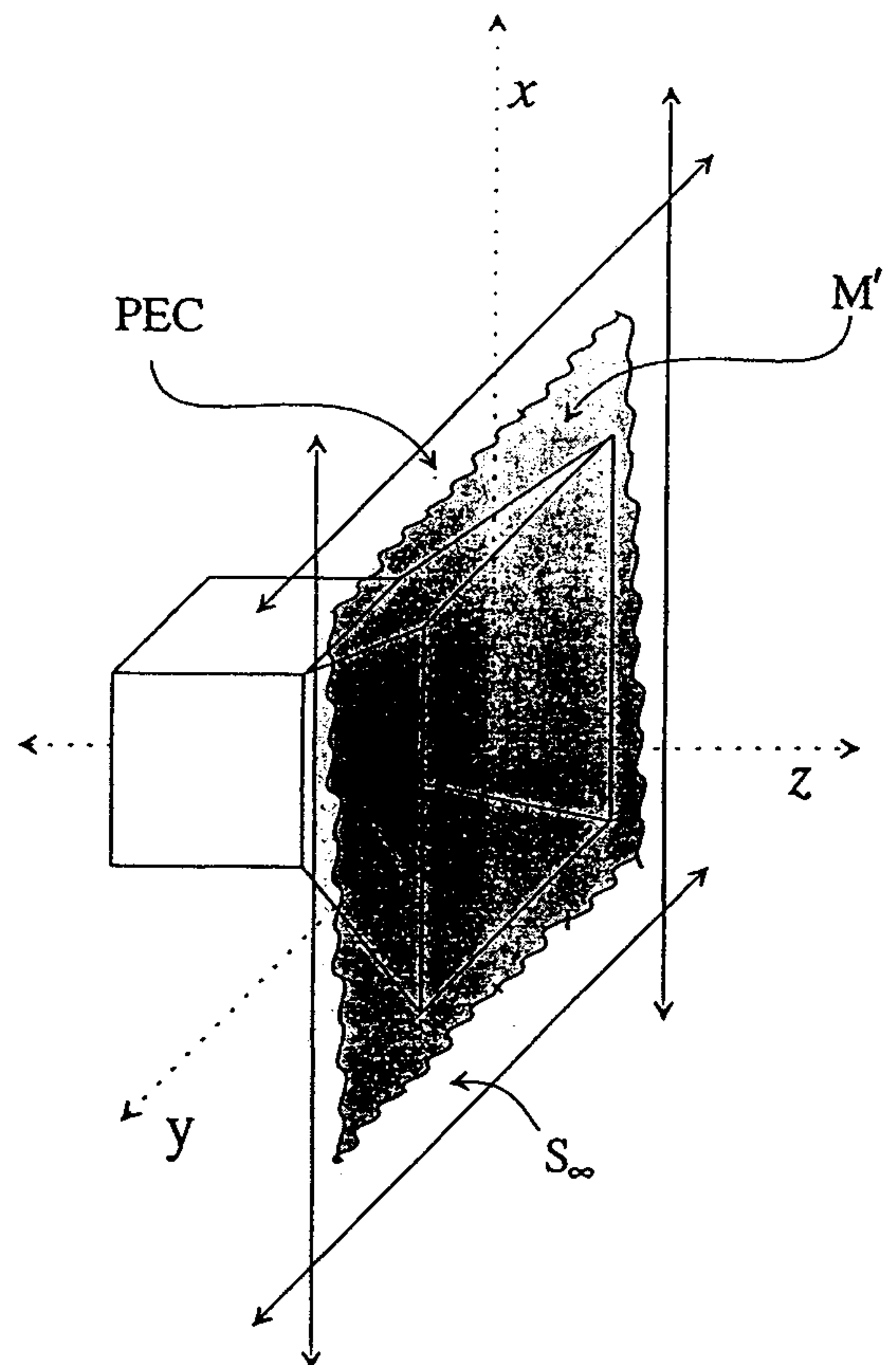


Fig. 1. Equivalent problem with a magnetic current sheet.

the method of least squares via singular value decomposition is presented in the following sections.

## II. FORMULATION OF THE ELECTRIC FIELD INTEGRAL EQUATION BY THE EQUIVALENT MAGNETIC CURRENT APPROACH

Consider an arbitrarily shaped antenna radiating into free space. The aperture of the antenna is in a plane surface separating all space into left half and right half spaces as shown in Fig. 1. The aperture of the antenna is placed in the  $xy$ -plane and is facing the positive  $z$ -axis. Since we are interested only in the electromagnetic field in front of the radiating antenna (i.e., the space where  $z > 0$ ), we place a perfect electric conductor, extending to infinity in the  $x$ - and  $y$ -directions, on the  $xy$ -plane in front of the aperture of the antenna (Fig. 1). By the equivalence principle [1], a surface magnetic current  $M'$  may be placed on this perfect electric conductor whose value is equal to the tangential value of the electric field on the  $xy$ -plane

$$M' = E \times \hat{n} \text{ on } S_\infty \quad (1)$$

where  $E$  is the electric field on the  $xy$ -plane,  $S_\infty$  is the entire  $xy$ -plane at  $z = 0$ , and  $\hat{n}$  is the unit outward normal to the  $xy$ -plane pointing in the direction of the positive  $z$ -axis.

Using image theory [1], an equivalent magnetic current  $M$  can be introduced as

$$M = 2M' \quad (2)$$

radiating in free space. Therefore,

$$M = 2E \times \hat{n} \text{ on } S_\infty \quad (3)$$

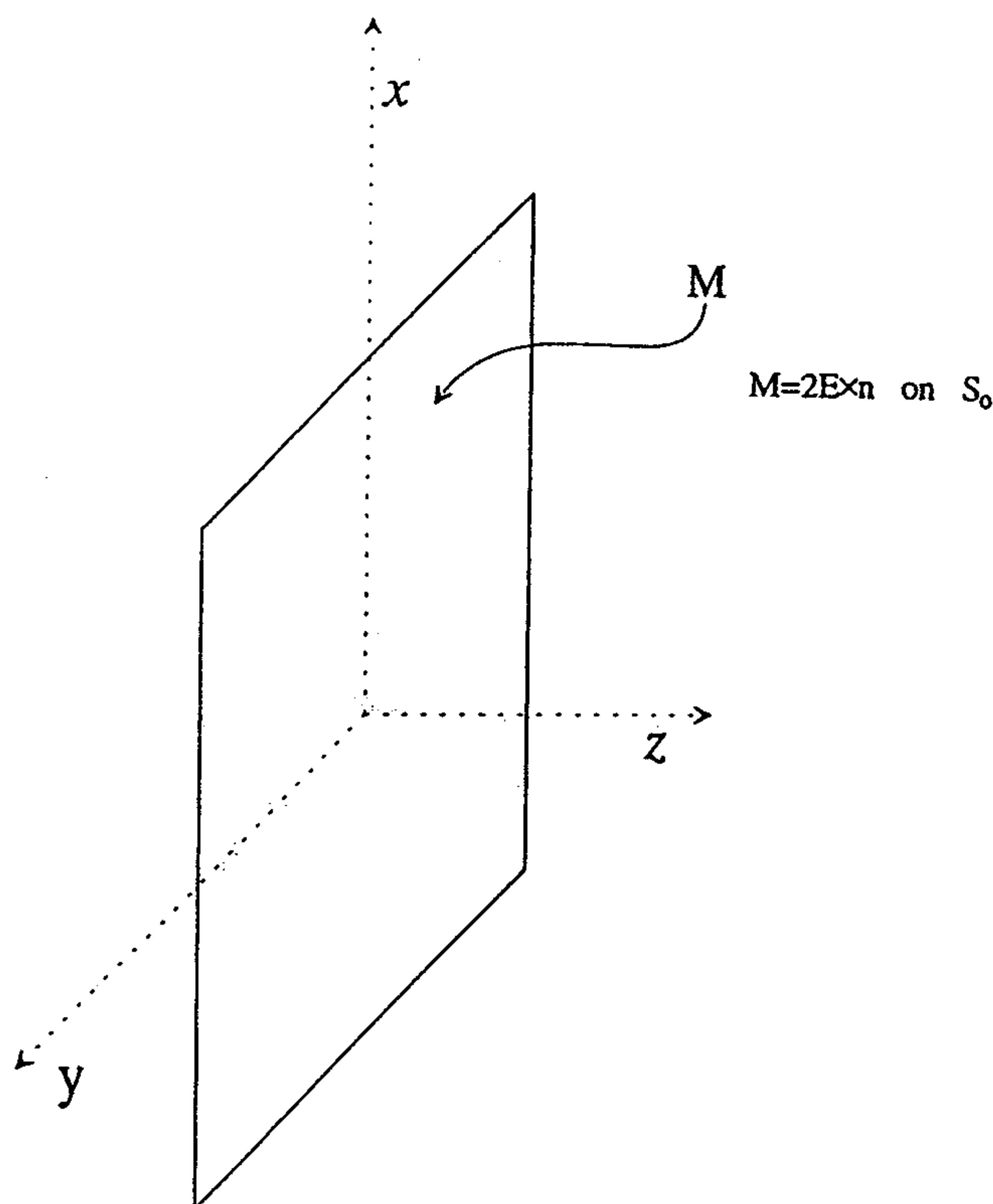


Fig. 2. Equivalent magnetic current covering the aperture of the antenna and radiating in free space.

where  $M$  now replaces the source antenna and radiates into free space (Fig. 2), producing exactly the same field as the original antenna in the region  $z > 0$ . The measured near field of the antenna may now be used to determine  $M$  from

$$E_{\text{meas}} = E(M) = -\frac{\nabla X}{4\pi} \int_{S_\infty} M(r') g(r; r') ds' \quad (4)$$

where  $E_{\text{meas}}$  is the electric near field measured over a geometry at a distance away from the aperture of the radiating antenna. Here  $r$  is the field location and  $r'$  is the location of the source point and  $\nabla$  is the gradient operator in the cartesian coordinates. In addition, the free space Green's function  $g(r; r')$  is given by

$$g(r, r') = \frac{e^{-jk_0|r-r'|}}{|r-r'|} \quad (5)$$

and  $k_0 = 2\pi/\lambda$  where  $\lambda$  is the wavelength.

By assuming that the measured field points are far from the current carrying region  $S_0$  ( $S_\infty$  is the truncated to  $S_0$  for numerical computation as per Fig. 2), the equivalent magnetic current  $\vec{M}$  can be expanded into Hertzian dipoles existing at the center of the 2-D patch as is conventionally done in the method of moments [5].

Therefore,

$$M_x(x', y') = \sum_{i=1}^{N_x} \sum_{j=1}^{N_y} \alpha_{ij} \Delta x \Delta y \delta(x' - x_i, y' - y_j) \quad (6a)$$

$$M_y(x', y') = \sum_{i=1}^{N_x} \sum_{j=1}^{N_y} \beta_{ij} \Delta x \Delta y \delta(x' - x_i, y' - y_j) \quad (6b)$$

where  $\alpha_{ij}$  and  $\beta_{ij}$  are the unknowns to be solved for. The effect of the  $\delta$ -functions in (6) is to replace the integrals in (4) by their

integrands evaluated at the positions of the  $\delta$ -functions. Since the electric near field is known at discrete points on the geometry over which it has been measured, a point matching procedure [5] is chosen. Substituting (6) into (4) and utilizing point matching, the following matrix equation is obtained

$$\begin{bmatrix} \vec{E}_{\text{meas}, \theta} \\ \vec{E}_{\text{meas}, \phi} \end{bmatrix} = \begin{bmatrix} H_{11} & H_{12} \\ H_{21} & H_{22} \end{bmatrix} \begin{bmatrix} \vec{M}_x \\ \vec{M}_y \end{bmatrix} \quad (7)$$

where  $\vec{E}_{\text{meas}, \theta}$  and  $\vec{E}_{\text{meas}, \phi}$  are column vectors whose elements are the  $\theta$ - and  $\phi$ -components of the electric near field, respectively, measured at discrete points.  $\vec{M}_x$  and  $\vec{M}_y$  are column vectors whose elements are the unknown coefficients  $\alpha_{ij}$  and  $\beta_{ij}$ , respectively.  $H_{11}$ ,  $H_{12}$ ,  $H_{21}$ , and  $H_{22}$  are the submatrices of the entire moment matrix and are given by

$$[H_{11}]_{k,l} = \left\{ \cos \theta_k \sin \phi_k \frac{e^{-jk_0 R_{k,l}}}{4\pi R_{k,l}^2} (z_k^f) \left[ jk_0 + \frac{1}{R_{k,l}} \right] + \sin \theta_k \frac{e^{-jk_0 R_{k,l}}}{4\pi R_{k,l}^2} (y_k^f - y_l^s) \left[ jk_0 + \frac{1}{R_{k,l}} \right] \right\} \Delta x \Delta y \quad (8a)$$

$$[H_{12}]_{k,l} = - \left\{ \cos \theta_k \cos \phi_k \frac{e^{-jk_0 R_{k,l}}}{4\pi R_{k,l}^2} (z_k^f) \left[ jk_0 + \frac{1}{R_{k,l}} \right] + \sin \theta_k \frac{e^{-jk_0 R_{k,l}}}{4\pi R_{k,l}^2} (x_k^f - x_l^s) \left[ jk_0 + \frac{1}{R_{k,l}} \right] \right\} \Delta x \Delta y \quad (8b)$$

$$[H_{21}]_{k,l} = \left\{ \cos \phi_k \frac{e^{-jk_0 R_{k,l}}}{4\pi R_{k,l}^2} (z_k^f) \left[ jk_0 + \frac{1}{R_{k,l}} \right] \right\} \Delta x \Delta y \quad (8c)$$

$$[H_{22}]_{k,l} = \left\{ \sin \phi_k \frac{e^{-jk_0 R_{k,l}}}{4\pi R_{k,l}^2} (z_k^f) \left[ jk_0 + \frac{1}{R_{k,l}} \right] \right\} \Delta x \Delta y \quad (8d)$$

where  $\theta_k$  and  $\phi_k$  are the  $\theta$  and  $\phi$  coordinates, respectively, of the  $k$ th field measuring point and  $x_l^s, y_l^s$  are the  $x$ - and  $y$ -coordinates,



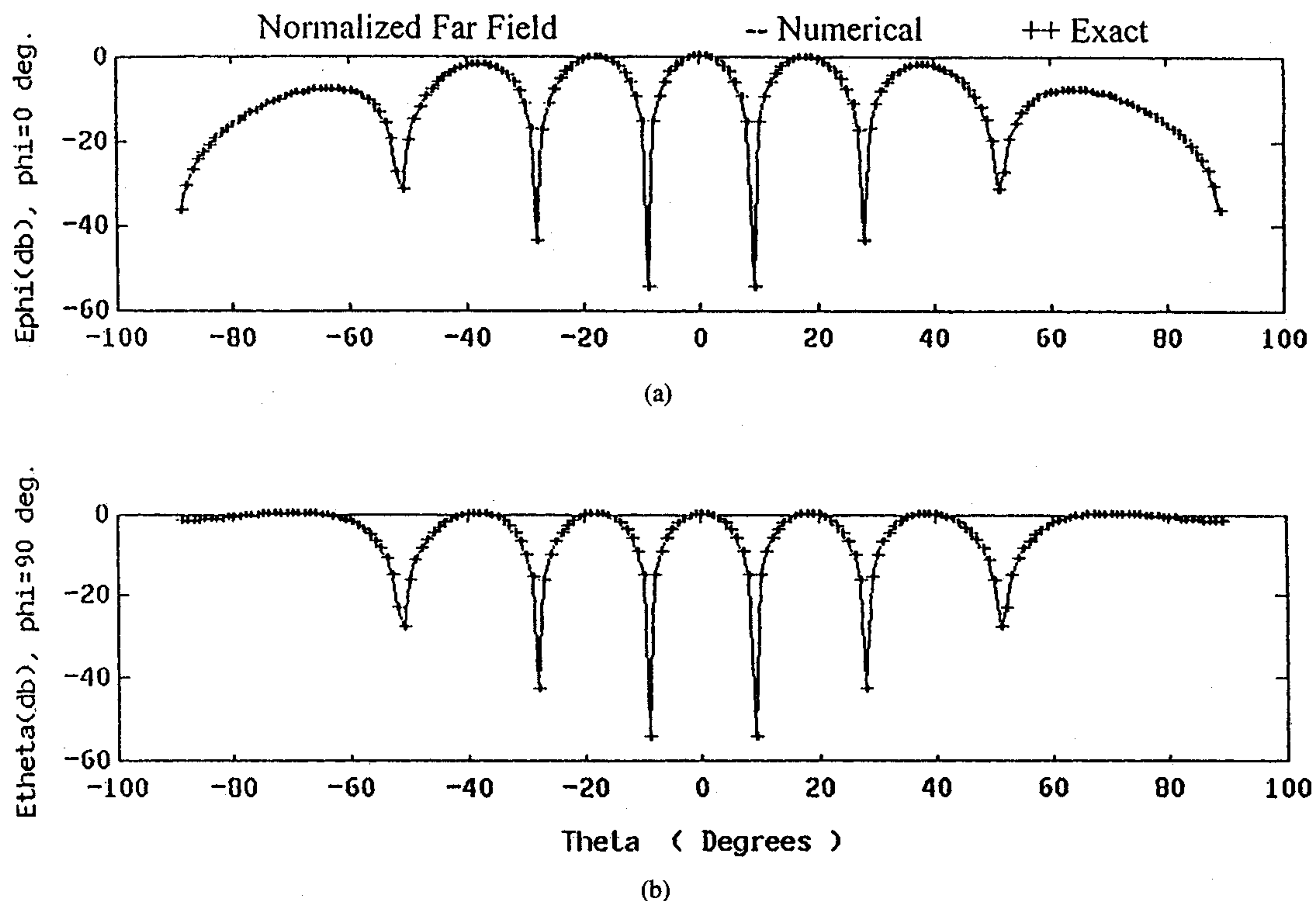


Fig. 3. (a) Comparison of exact and computed far field  $\phi = 0^\circ$  and  $90^\circ$  cut for a  $2 \times 2$  electric dipole array on a  $3.6\lambda \times 3.6\lambda$  surface. (b) Near field was measured on an arc.

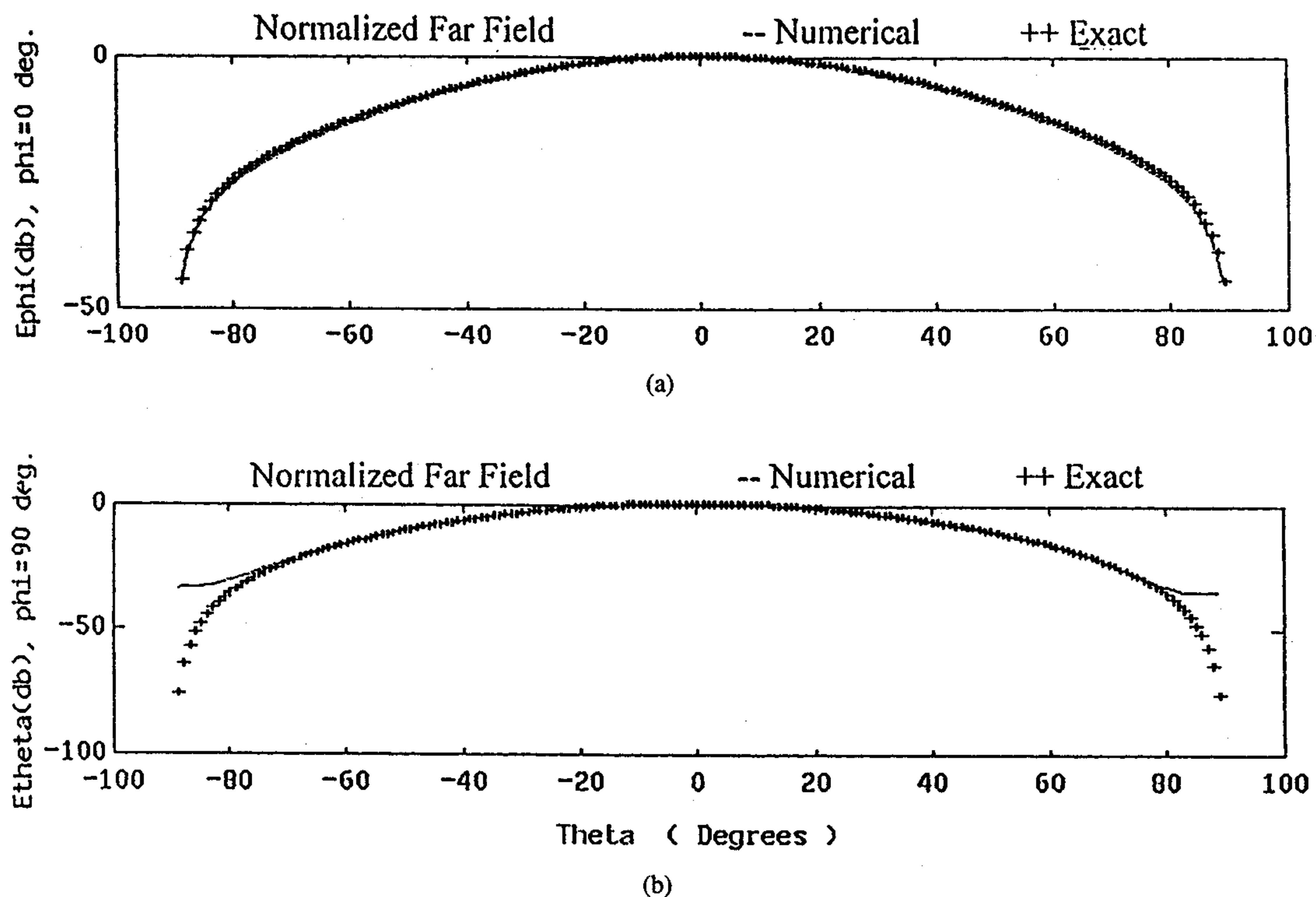


Fig. 4. (a) Comparison of exact and computed far fields ( $\phi = 0^\circ$ ) for sinusoidal magnetic excitation on a  $1\lambda \times 1\lambda$  surface. Near field was measured on a straight line parallel to the  $x$ -axis, extending to  $\pm 9\lambda$  and crossing  $z = 3\lambda$ . (b) Comparison of exact and computed far fields ( $\phi = 90^\circ$ ) for sinusoidal magnetic excitation on a  $1\lambda \times 1\lambda$  surface. Near field was measured on a straight line parallel to the  $x$ -axis, extending to  $\pm 9\lambda$  and crossing  $z = 3\lambda$ .

respectively, of the  $l$ th source point.  $R_{k,l}$  is the distance between the  $k$ th field point ( $r_k$ ) and the  $l$ th source point ( $r_l^s$ )

$$R_{k,l} = \sqrt{(x_k^f - x_l^s)^2 + (y_k^f - y_l^s)^2 + (z_k^f)^2}. \quad (9)$$

The superscript  $f$  denotes the field measuring point and the superscript  $s$  denotes the source point. Note that in (8) the two subscripts  $i$  and  $j$  have been replaced by the single subscript  $l$ . That is,  $(x_l^s, y_l^s)$  is  $(x_i, y_j)$  where  $i$  and  $j$  are determined by  $l$ .  $\Delta x$  and  $\Delta y$  represent the size of the patch on  $S_o$  carrying the dipoles.

The resulting matrix (7) with (8), when solved, determines the elements of  $\vec{M}_x$  and  $\vec{M}_y$ . This matrix equation is solved using the method of total least squares with singular value decomposition [4].

### III. NUMERICAL RESULTS

In this section, use is made of both synthetic and experimental near field data. An attempt is made to illustrate the accuracy of the method presented here for near-field to near/far-field transformation. The results will include experiments with different antenna configurations as well as near field data taken over various geometries. As a first example, consider a four-dipole array placed at the corners of a  $3.6\lambda$  by  $3.6\lambda$  planar surface on the  $xy$ -plane. The center of the  $3.6\lambda \times 3.6\lambda$  surface is located at  $(x = 0, y = 0)$ . At a spherical distance of  $3\lambda$  from the origin with  $0^\circ < \theta < 30^\circ$  and  $0^\circ < \phi < 360^\circ$ , on 200 discrete points, both the electric field components  $E_\theta$  and  $E_\phi$  are computed analytically. A fictitious planar surface in the  $xy$ -plane of dimensions  $4\lambda \times 4\lambda$  is used to form a planar magnetic current sheet. This magnetic current sheet is divided into  $10 \times 10$  magnetic current patches. The values of these currents were determined using synthetically computed near field data and choosing 114 singular values for the moment matrix. Fig. 3 compares the absolute value of the electric far-field components computed by the present method, with the exact far field computed analytically. Fig. 3(a) presents  $E_\phi$  in db for  $\phi = 0^\circ$  as a function of  $\theta$ , and Fig. 3(b) presents  $E_\theta$  in db for  $\phi = 90^\circ$ . The comparison is visually indistinguishable. The cross polar components are negligible. Next, consider an antenna with a sinusoidal excitation. The aperture of the antenna is a square with dimension  $a = 1\lambda$ , whose center is placed at  $(x = 0, y = 0)$ . The excitation is  $x$ -directed and given by

$$\begin{cases} \sin\left(\frac{\pi}{2} + \frac{\pi x}{a}\right) & \text{for } \left| \begin{array}{l} -\frac{a}{2} \leq x \leq \frac{a}{2} \\ -\frac{a}{2} \leq y \leq \frac{a}{2} \end{array} \right| \\ 0. & \text{otherwise} \end{cases}$$

The near field geometry chosen for this experiment is a straight line parallel to the  $x$ -axis, extending to  $\pm 9\lambda$  and crossing  $z = 3\lambda$ . The electric field components  $E_\theta$  and  $E_\phi$  have been computed analytically along this straight line at intervals of  $0.01\lambda$ . A fictitious planar surface in the  $xy$ -plane of dimensions  $1\lambda \times 1\lambda$  is used to form a planar magnetic current sheet. This magnetic current sheet is divided into  $10 \times 10$  equally spaced magnetic current patches. The value of these currents were determined using synthetically computed near field data, and choosing 428 singular values for the moment matrix. Fig. 4(a) and (b) compare the absolute value of the electric far field computed by the equivalent magnetic current approach with the exact far field computed analytically. Fig. 4(a) presents  $E_\phi$  in db for  $\phi = 0^\circ$  as  $\theta$  varies from  $-90^\circ$  to  $90^\circ$  and, as shown, the comparison is excellent. Fig. 4(b) presents  $E_\theta$  for  $\phi = 90^\circ$  as a function of  $\theta$ . As observed, for  $\theta$  values up to  $\pm 76^\circ$ , the agreement is very good. The reason for the discrepancy beyond  $76^\circ$  is that this cut is in a principal plane perpendicular to the plane where the near field was measured, and since we are using a straight line for the near field geometry, there is not enough information in the measured near field to correctly predict the far-field pattern for  $\theta$  beyond  $\pm 76^\circ$ . Next, consider an antenna with a circular aperture radiating a  $TE_{11}$  mode in space. The plane of the circular aperture is on the  $xy$ -plane centered at  $(x = 0.2\lambda, y = 0)$  with radius  $0.5\lambda$ . The excitation is

$$\vec{M} = \left[ \frac{x_{11}}{a} J_0\left(\frac{x_{11}}{a}\rho\right) - \frac{1}{\rho} J_1\left(\frac{x_{11}}{a}\rho\right) \right] \cos\phi \hat{\rho} - \frac{1}{\rho} J_1\left(\frac{x_{11}}{a}\rho\right) \sin\phi \hat{\phi}$$

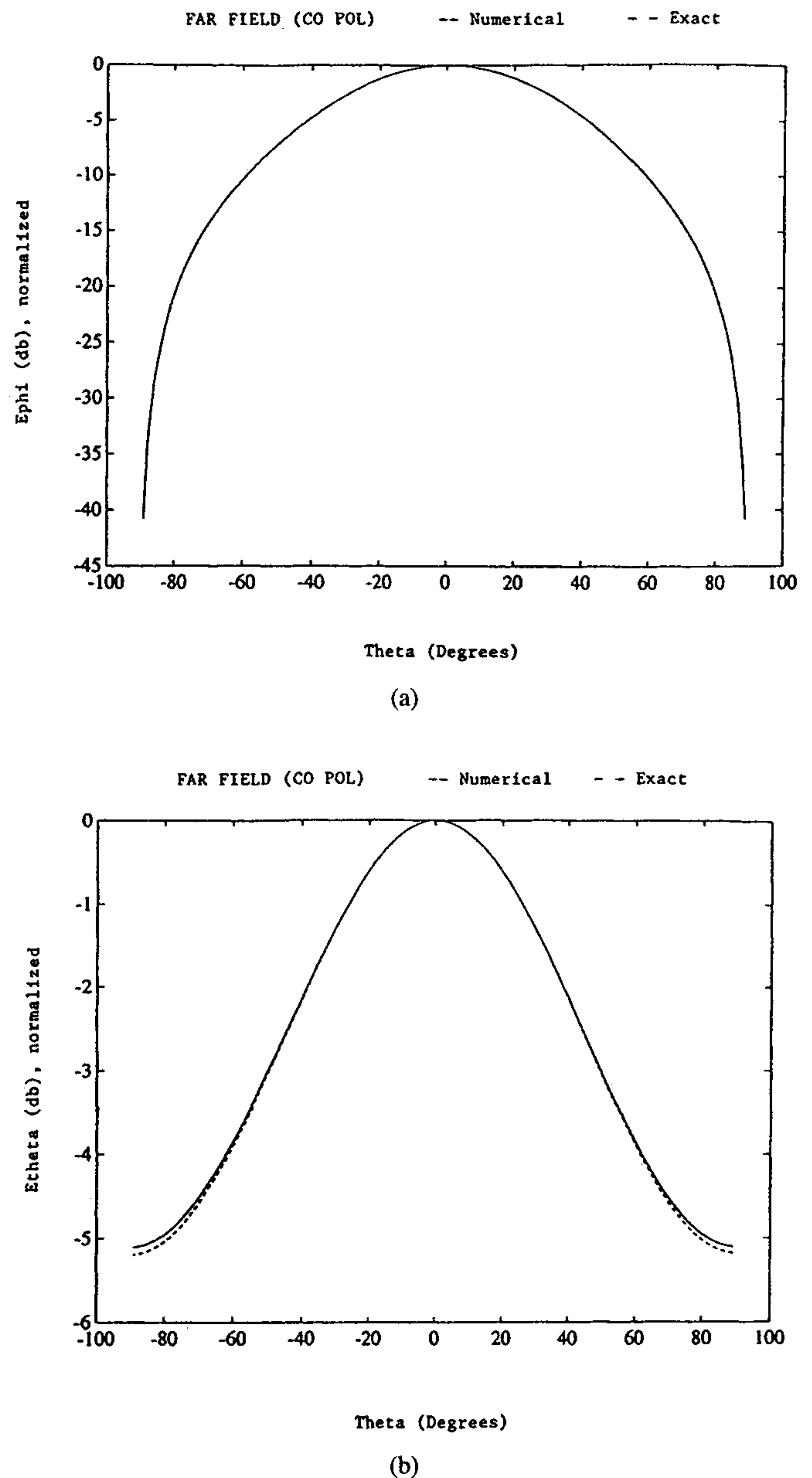


Fig. 5. (a) Comparison of exact and computed far fields ( $\phi = 0^\circ$ ) for circular aperture. (b) Comparison of exact and computed far fields ( $\phi = 90^\circ$ ) for circular aperture.

where  $x = 1.841$ ,  $J_0$  and  $J_1$  are the zero and first-order Bessel functions. The near field geometry chosen for this experiment is a hemispherical surface with  $r = 3\lambda$ ,  $0 \leq \theta \leq 90^\circ$ , and  $0 \leq \phi \leq 360^\circ$ . The simulated aperture chosen for the experiment is a rectangle with dimensions  $1.5\lambda \times 1.5\lambda$  divided into  $20 \times 20$  equally spaced magnetic current patches, the number of field points chosen for this experiment were 1200, and 560 singular values were chosen for the moment matrix. The copolarization patterns of the far fields obtained are depicted in Fig. 5(a) and (b). The results are compared with exact solution and, as observed, the comparison is good.

Next, experimentally measured data is utilized. Consider a microstrip array consisting of  $32 \times 32$  uniformly distributed patches on a  $1.5\text{m} \times 1.5\text{m}$  surface. The near fields are measured at discrete points on a spherical surface at a distance 1.23 m away from the antenna at a frequency of 3.3 GHz. The data is taken every  $4^\circ$  in  $\phi$  for  $0^\circ \leq \phi \leq 360^\circ$  and every  $2^\circ$  in  $\theta$  for  $0^\circ \leq \theta \leq 90^\circ$ . Measurements have been



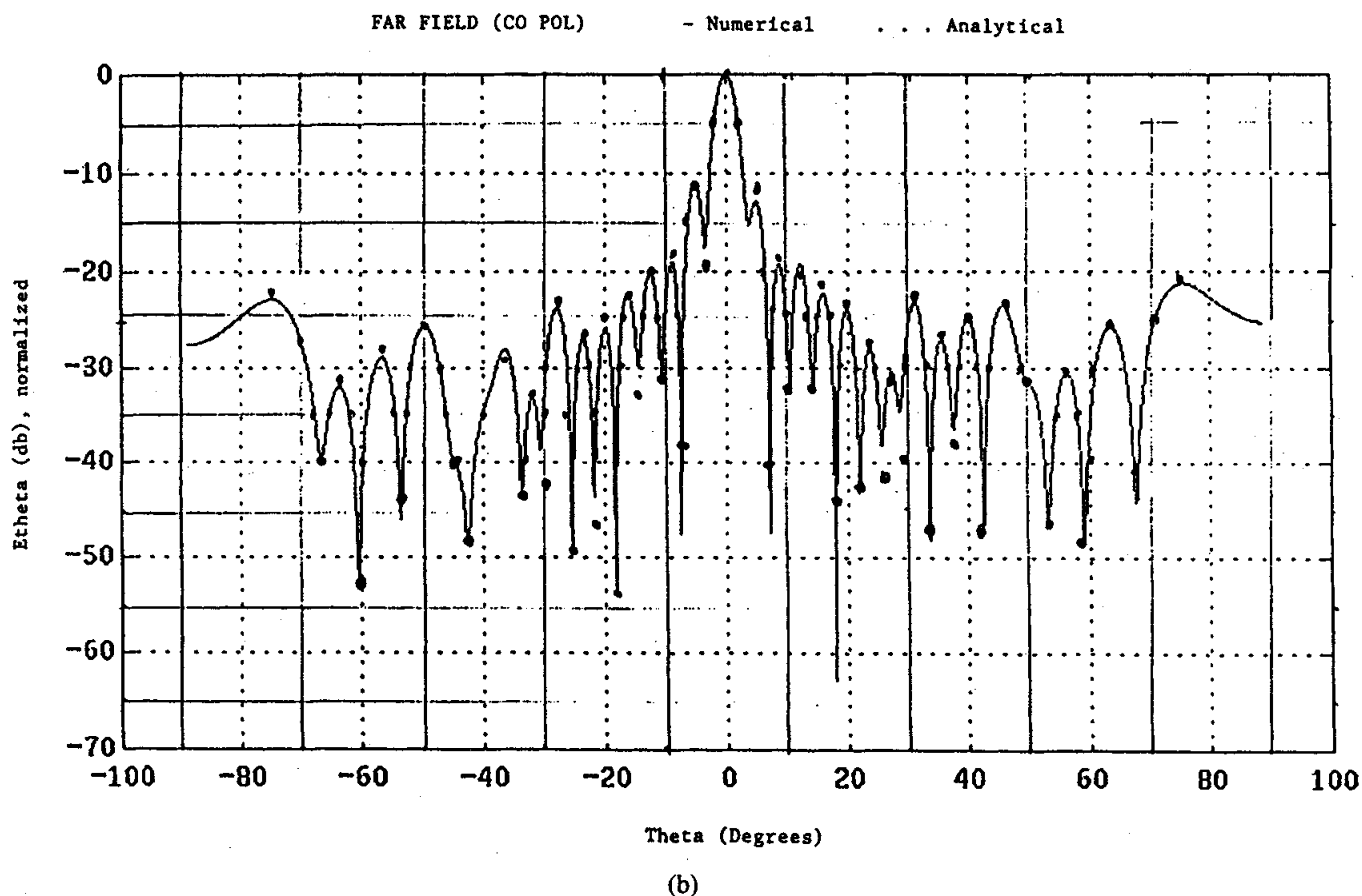
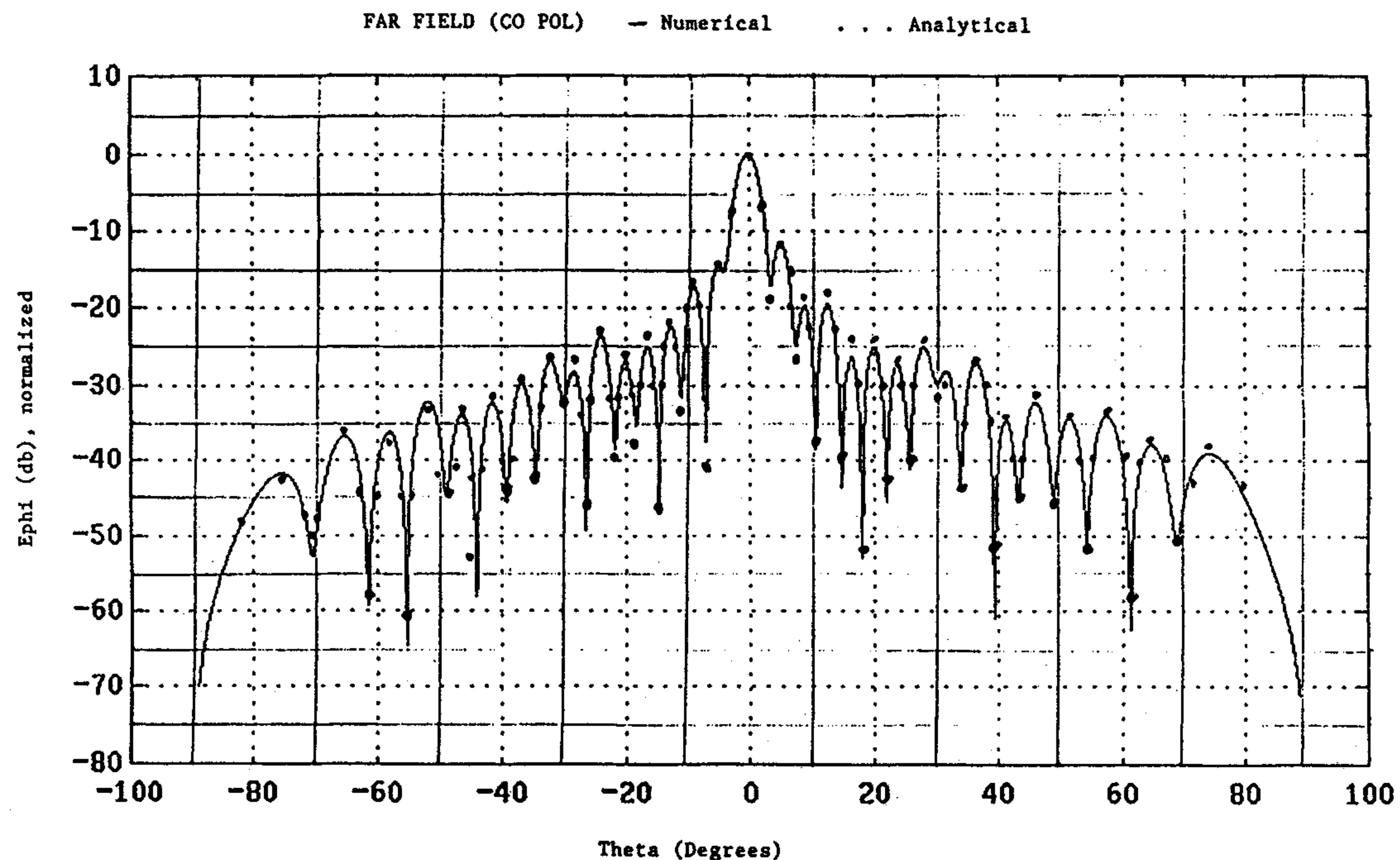
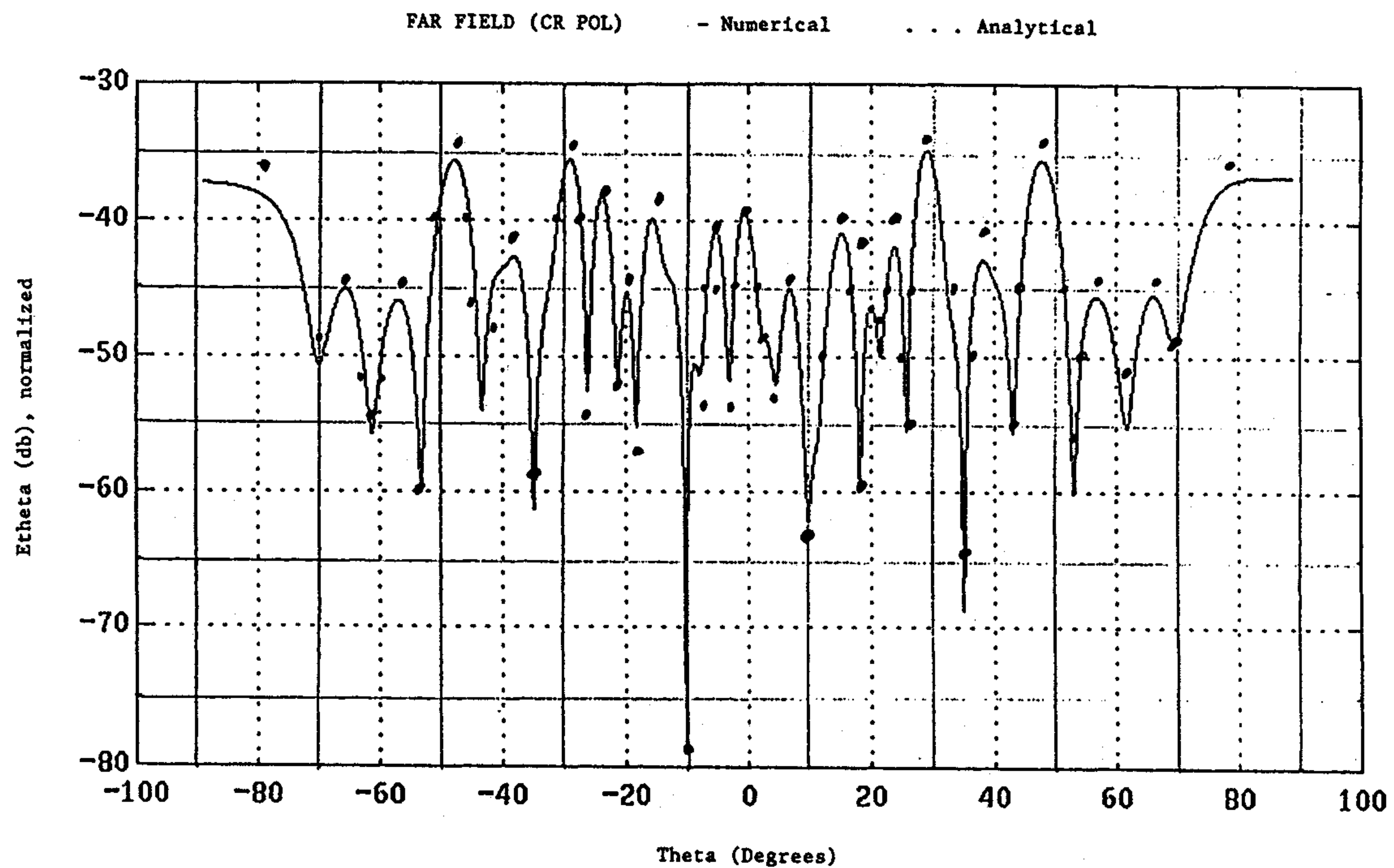


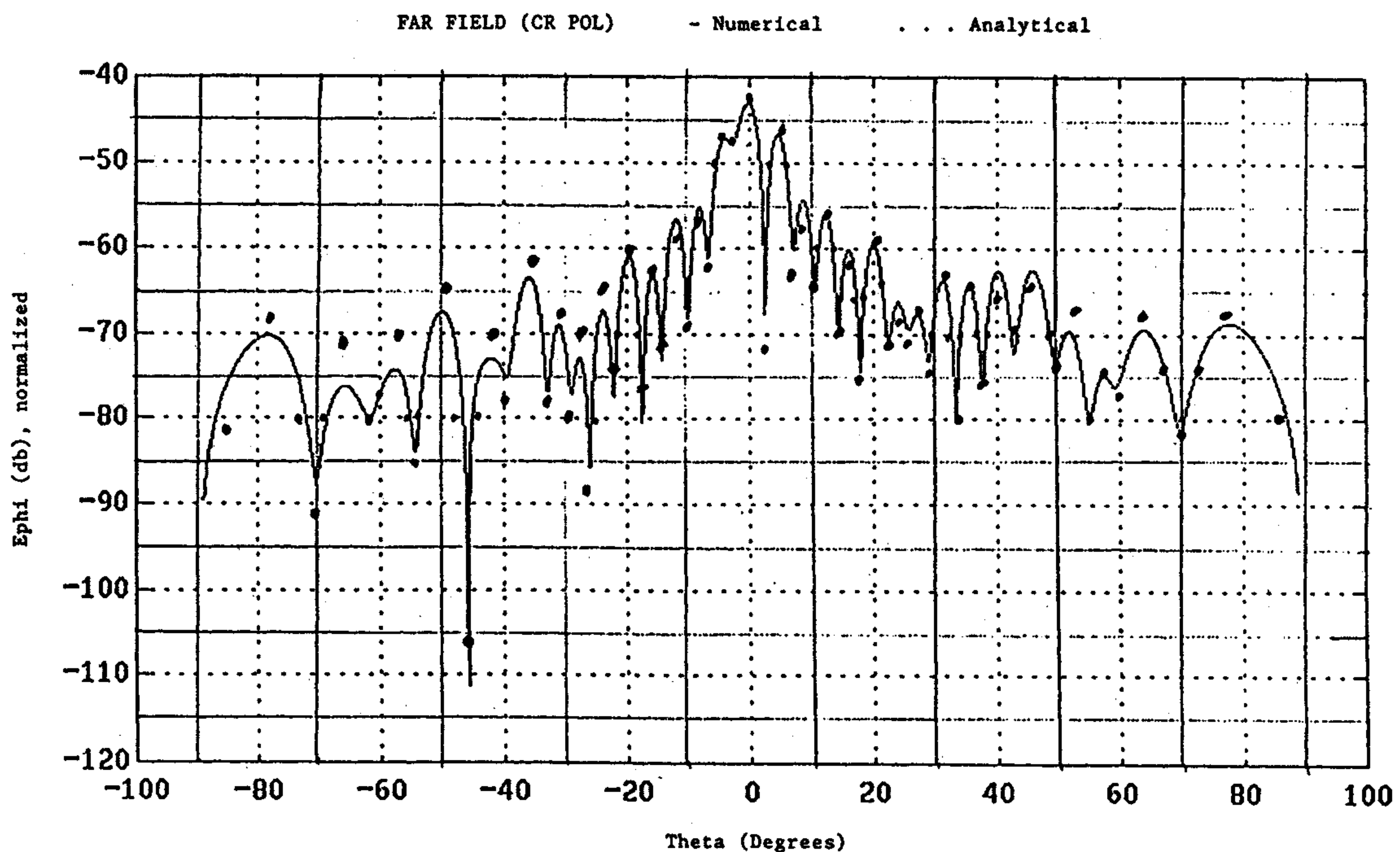
Fig. 6. (a) Copolarization characteristic for  $\phi = 0^\circ$  cut for a  $32 \times 32$  patch microstrip array using numerical and analytical results. (b) Copolarization characteristic for  $\phi = 90^\circ$  cut for a  $32 \times 32$  patch microstrip array using numerical and analytical results.

performed using an open ended cylindrical WR284 wave guide with the  $TE_{11}$  as the dominant mode of propagation. The measured data was provided by Dr. C. Stubenrauch of NIST. In Fig. 6, a fictitious planar surface on the  $xy$ -plane of dimensions  $1.9\text{m} \times 1.9\text{m}$  is used to form a magnetic current sheet. This magnetic current sheet is divided into  $49 \times 49$  equally spaced magnetic current patches,  $0.33\lambda$  apart. This figure compares the copolarization characteristic of the electric far-field pattern  $E_\phi$  obtained by the present method with the result obtained numerically. These numerical results are the result of

near-field to far-field transformation using spherical wave expansions where the fields are expanded in terms of TM and TE to  $r$  modes. Fig. 6(a) describes  $20 \log_{10} |E_\phi|$  for  $\phi = 0^\circ$  and  $-89^\circ \leq \theta \leq 89^\circ$ . Near field data was measured on 8100 discrete points located on the surface of a hemisphere at a radius of 1.23 m from the center of the antenna's aperture, and 4230 singular values were chosen for the moment matrix. Fig. 6(b) depicts the copolarization characteristic of the electric far field for  $\phi = 90^\circ$ , and the same effects as before are observed. Fig. 6(c) and (d) describe the cross-polarization



(c)



(d)

Fig. 6. (Continued.) (c) Cross-polarization characteristic for  $\phi = 0^\circ$  cut for  $32 \times 32$  patch microstrip array using numerical and analytical results. (d) Cross-polarization characteristic for  $\phi = 90^\circ$  cut for  $32 \times 32$  patch microstrip array using numerical and analytical results.

characteristics of the far-field patterns. Fig. 6(c) depicts  $20 \log_{10} |E_\phi|$  for  $\phi = 90^\circ$  and  $-89^\circ \leq \theta \leq 89^\circ$ .

#### IV. CONCLUSION

The method presented here determines the fields for  $z > 0$  in front of the radiating antenna simply from the knowledge of the near field on any arbitrary geometry in space. Using various antenna configurations and near-field geometries, an investigation of the accuracy of this method was performed. For cases where

synthetic sources were used, the far fields were compared with exact solutions and the agreements were quite good. For cases where actual experimental sources were used, the far fields were compared with a semi-analytical approach.

#### REFERENCES

- [1] P. Petre and T. K. Sarkar, "Planar near field to far-field transformation using an equivalent magnetic current approach," *IEEE Trans. Antennas Propagat.*, vol. 40, pp. 1348-1356, Nov. 1992.

- [2] R. F. Harrington, *Field Computation by Moment Methods*. Melbourne, FL: Krieger, 1987.
- [3] G. H. Golub and C. F. Van Loan, *Matrix Computations*. Baltimore, MD: Johns Hopkins University Press, 1989, 2nd ed.
- [4] J. Rahman and T. K. Sarkar, "Deconvolution and total least squares in finding the impulse response of measured data from electromagnetic system," *IEEE Trans. Antennas Propagat.*, vol. 43, pp. 416-421, Apr. 1995.
- [5] P. Petre and T. K. Sarkar, "Planar near-field to far-field transformation using an array of dipole probes," *IEEE Trans. Antennas Propagat.*, vol. 42, pp. 534-537, Apr. 1994.